Continental Shelf Research 69 (2013) 38–51

Contents lists available at ScienceDirect

Continental Shelf Research

journal homepage: www.elsevier.com/locate/csr

Research papers

The use of circulation weather types to predict upwelling activity along the western Iberian Peninsula coast

Alexandre M. Ramos [a,*], Ana Cordeiro Pires [b], Pedro M. Sousa [a], Ricardo M. Trigo [a]

[a] Instituto Dom Luiz, Faculdade de Ciências, Universidade de Lisboa, Portugal
[b] Centro de Estudos do Ambiente e do Mar (CESAM) & Departamento de Física, Universidade de Aveiro, Portugal

A R T I C L E I N F O

Article history:
Received 6 November 2012
Received in revised form
5 August 2013
Accepted 30 August 2013
Available online 17 September 2013

Keywords:
Upwelling
Circulation weather types
Western Iberian Peninsula
Statistical model
Prediction

A B S T R A C T

Coastal upwelling is a phenomenon that occurs in most western oceanic coasts, associated with coastal surface water divergence and consequent ascension of colder and nutrient-rich waters from deeper levels. In this work, we evaluate the intra- and interannual variability of the upwelling index (UI) off the western coast of the Iberian Peninsula considering six locations at various latitudes along the 10°W meridian: Rias Baixas (42°N), Aveiro (41°N), Figueira da Foz (40°N), Cabo da Roca (39°N), Sines (38°N) and Sagres (37°N). In addition, the relationship between the variability of the occurrence of several circulation weather types (CWTs) and the UI variability along this coast was assessed in detail, allowing to discriminate which types are frequently associated with strong and weak upwelling activity. It is shown that upwelling activity is mostly driven by wind flow from the northern quadrant, for which the obtained correlation coefficients (for the N and NE types) are higher than 0.5 for the six considered locations.

Taking into account these significant relationships, we then developed statistical multi-linear regression models to hindcast upwelling series (April–September) at the referred locations, using monthly CWTs frequencies as predictors. Modeled monthly series reproduce quite accurately observational data, explaining more than 60% of the total variance, presenting skill-scores against the climatology also above 60%, and having relatively small absolute errors. However, despite the ability of our models in representing the interannual variability of UI, they do not reproduce accurately most UI peaks, that occur typically in July. This may be due to the role played by mesoscale phenomena not represented in the statistical models, namely sea breezes that result from the intensified thermal low, which enhances coastal meridional winds and hence upwelling.

1. Introduction

Classifications of atmospheric circulation have been developed to reduce the continuum of atmospheric circulation patterns into a reasonable and manageable number of discrete classes (Huth et al., 2008). Different methods exist for the classification of Circulation Weather Types (CWTs), as was shown by Huth et al. (2008), and Philipp et al. (2010).

Most CWTs classifications are developed for a specific region and result from the examination of synoptic weather data, usually on regular gridded fields, often based on sea level pressure or geopotential height at 500 hPa (Yarnal, 1992). They are typically defined for each day or group of consecutive days as a simple way to reflect the local circulation that actually occurred (e.g. Hess and Brezowsky, 1952; Kruizinga, 1979; Jones et al., 1993; Philipp et al., 2007). The use of objective methods to classify CWTs, such as those based on indices derived from atmospheric pressure fields, represent an advantage over more subjective studies of CWTs such as Lamb Weather Type (LWT) classification (Lamb, 1972) and the Grösswetterlagen catalogs (Hess and Brezowsky, 1977). Objective classification schemes, based on circulation indices, were initially developed for the British Isles (Jenkinson and Collison, 1977; Jones et al., 1993) in order to automatically reproduce the subjective LWT classification.

In recent years, the usefulness of CWTs classifications has been investigated for a wide range of applications, in scientific domains from climate (e.g. Ramos et al., 2010; Lorenzo et al., 2011), to environmental areas such as air quality (e.g. Demuzere et al., 2008) and forest fires (Kassomenos, 2010), to extreme events such as floods (e.g. Prudhomme and Genevier, 2011), droughts (e.g. Paredes et al., 2006; Vicente-Serrano et al., 2011), lightning activity (e.g. Ramos et al., 2011) or even avalanches (Esteban et al., 2005). Furthermore, several studies discuss that changes in the climate variables at the Earth's surface are usually a result of changes in the frequency of occurrence of CWTs (e.g. Fowler and Kilsby, 2002; Goodess and Palutikof, 1998; Kysely, 2008; Jones and Lister, 2009).

In this study, we used an automated version of synoptic CWTs that was initially developed for the British Isles (Jones et al., 1993),

* Correspondence to: Instituto Dom Luiz, Faculdade de Ciências, Universidade de Lisboa, Campo Grande, Edf. C8, Piso 3, Sala 8.3.1, 1749-016 Lisboa, Portugal. Tel.: +351 217500863.
E-mail address: amramos@fc.ul.pt (A.M. Ramos).

0278-4343/$ - see front matter
http://dx.doi.org/10.1016/j.csr.2013.08.019

and later adapted with success to western Iberian Peninsula (Trigo and DaCamara, 2000; Ramos et al., 2010). This classification describes the regional atmospheric circulation in terms of a small set of relatively simple circulation parameters.

The Iberian Upwelling System (IUS) occurs on the western coast of the Iberian Peninsula, corresponding to the northern limit of the Eastern North Atlantic Upwelling System, prolonged to the south by the Canary Upwelling System (Barton et al., 1998). Coastal upwelling is a phenomenon that occurs at the western coasts of continental masses due to the presence of the mid-latitude high-pressure systems over the ocean that generate equatorward winds along the eastern boundary of the ocean basin. In the Northern Hemisphere, southward winds along any continental western coast can induce, through the Coriolis effect, an offshore advection of water from the upper layers. This flow in turn gives origin to an equatorward current due to the tilt of the sea level consequent of coastal divergence, and this gives rise to the upwelling of colder and nutrient-rich waters from deeper layers (e.g. Wooster et al., 1976). On the contrary, during periods without upwelling, the prevailing circulation at the western Iberian Peninsula coast is a northward current in the upper layers (Haynes and Barton, 1990; Frouin et al., 1990). The Eastern North Atlantic Upwelling System is one of the four major upwelling systems of the world, including California (USA western coast), Humboldt (off the coasts of Peru and Chile) and Benguela (off southwestern Africa) (e.g. Chavez and Messié, 2009). These regions are the most biologically productive regions of the world ocean and crucial for fisheries, due to the phytoplankton blooms associated with the enrichment of the surface waters with nutrients from below (e.g. Pauly and Christensen, 1995).

In the western Iberian sector, the atmospheric and oceanic circulation and hydrology undergo strong seasonality. The Azores High generally migrates northward in late spring and summer, positioning itself just off the Iberian Peninsula, and giving rise to northerly, upwelling-favorable winds typically between May and September (Fiúza, 1983). These intense winds occur in episodes or events, acting over the ocean surface for several days at a time, but alternating with relaxation periods, where winds weaken or are rather south- or southwest-oriented (Peliz et al., 2002). After about 1 day of northerly winds acting over the ocean surface, the band of cold water begins to form at the coast, eventually producing finger-like structures called filaments that spread west and southwest (Haynes et al., 1993). These upwelling events in the IUS have been thoroughly characterized, both in terms of their main physical processes (Fiúza et al., 1982; Álvarez-Salgado et al., 1993; Peliz et al., 2002; Torres and Barton, 2007) as well as some of the associated biological processes (Santos et al., 2001; Queiroga et al., 2007; Arístegui et al., 2009; Oliveira et al., 2009). However, upwelling events depend not only on large-scale atmospheric circulation, but also on the coastal ocean mesoscale variability (e.g. Relvas et al., 2007, 2009) as well as on interannual to interdecadal atmospheric variability, detailed next.

Due to their importance in the maintenance of the associated marine ecosystems, upwelling regions have been the subject of study for the assessment of long-term trends and significant changes in past decades. One of the first important works on this matter was that of Bakun (1990), where the four upwelling systems were under scope and, based on observations for period 1946–1988, the author found that all systems showed an alongshore wind stress intensification trend during summer, which would implicate an upwelling intensification. Regarding a more regional scale and for a longer period, Lemos and Pires (2004) found a weakening trend for the longer 1941–2000 period for western Iberian Peninsula when analyzing both meridional wind component and SST datasets, although punctuated by strong interannual variability. The analysis of annual or seasonal signal tendency may hide different behaviors at the monthly scale. Thus, Alvarez et al. (2008) confirmed this negative tendency for period 1967–2006 for months March, April and July–December, but found a positive trend for the remaining months, concluding that there is no clear seasonal trend in upwelling intensity in past decades. On the other hand, Santos et al. (2005), based on a shorter satellite-based SST dataset, reported an upwelling regime shift in the early 1990s to stronger upwelling events, after a positive maximum of the North Atlantic Oscillation (NAO) winter index, corroborated by stronger coastal zonal gradients in summer from 1992 onwards. Furthermore, Borges et al. (2003) found a higher frequency in northerly wind occurrence during winter, and consequently an increase in winter upwelling events. Santos et al. (2011) also studied the dependence of upwelling trends (western coast of the Iberian Peninsula) taking into account different fitting trend methodologies. The difficulty to assess trends of upwelling activity has been summarized recently when Narayan et al. (2010) showed that there can be large discrepancies when analyzing trends derived from upwelling indicators (wind stress and SST), with both depending on the dataset used.

The major aims of this paper are twofold: first to study the relationship between the CWTs and upwelling variability along the western coast of the Iberian Peninsula and secondly to develop statistical models to hindcast upwelling series, using frequencies of CWTs as predictors. The remainder of the paper is organized as follows: in Section 2, different data sets and the methodologies used in the analysis are described. In Section 3.1 we characterized the seasonal and interannual distribution of the upwelling index in the western coast of the Iberian Peninsula, while in Section 3.2 we characterize in detail the circulation weather types and its variability. In Section 3.3 we studied the relationship between the upwelling index and circulation weather types and in Section 3.4 the statistical modeling of the upwelling index by means of circulation weather types frequencies is presented. Finally, Section 4 concludes.

2. Data and methods

2.1. Upwelling index

The upwelling index (UI) is a measure of occurrence of upwelling. There are, in general, two ways to compute this quantity, both already used for the IUS: (1) the Ekman transport perpendicular to the coastline, that is, generated by the alongshore wind stress component (e.g. Alvarez et al., 2008); and (2) the difference between coastal (10–50 km) and oceanic ($\sim$500 km) SST (e.g. Santos et al., 2005). Both methods have advantages and caveats and some of these are discussed here. The first method, despite being based on the known effect of wind stress over the ocean surface and adjacent layers, which is the main driver of upwelling, does not account for the effects of capes and other coastal features, or mesoscale phenomena of which upwelling is also dependent on (Peliz et al., 2002; Relvas et al., 2009). The second approach is more of a proxy for upwelling occurrence, since upwelling is not the only cause for offshore–onshore SST differences; SST is strongly influenced by other phenomena such as river discharge in coastal areas and large-scale circulation offshore (Gómez-Gesteira et al., 2008).

In this study, the UI was provided by the Spanish Institute of Oceanography (IEO—http://www.indicedeafloramiento.ieo.es) and was computed by means of geostrophic winds following the method by Bakun (1973) and adapted later to the Iberian Peninsula by Lavín et al. (1991, 2000) (see formulation used by IEO below). The geostrophic winds were computed from 6-hourly atmospheric sea level pressure (SLP) fields (at a 1° resolution) obtained from the U.S. Navy Fleet Numerical Meteorology and Oceanography Center (FNMOC) for the 1967–2011 period. The use of the FNMOC SLP fields to compute the UI index has been used widely in different studies (e.g. Bograd et al., 2009; Macías et al.,

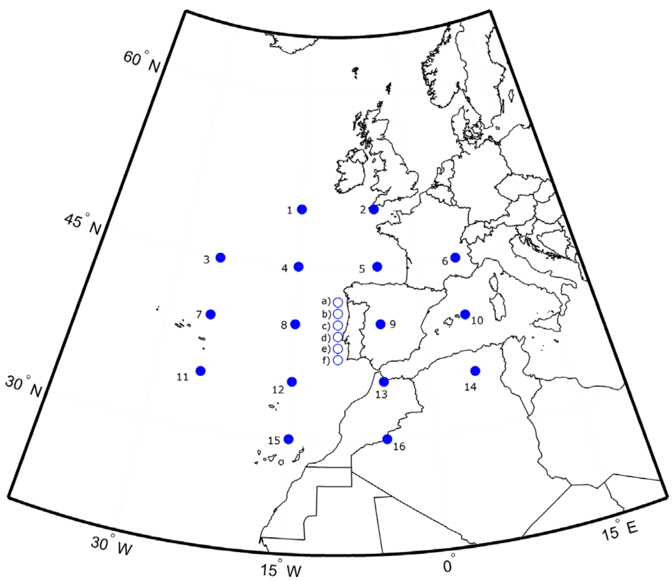

Fig. 1. Location of the 16 grid points (1–16) used to compute the geostrophic (vorticity and directional flow) indices. In addition, the location of the six upwelling indexes along the 10°W meridian is also shown for (a) Rias Baixas (42°N); (b) Aveiro (41°N); (c) Figueira da Foz (40°N); (d) Cabo da Roca (39°N); (e) Sines (38°N); and (f) Sagres (37°N).

2012) and namely for western Iberia, Alvarez et al., 2011. Given the almost meridional character of the western coast of the Iberian Peninsula (Fig. 1), UI can be formulated solely taking into account the cross-shore component of the Ekman transport

$$UI = -\frac{\tau_y}{\rho_{sw} f}$$

where $\tau_y = \rho_a C_d \sqrt{u^2+v^2}\, v$ is the meridional wind stress component ($\rho_a \approx 1.22\ \mathrm{kg\ m^{-3}}$ is the air density, C_D is an adimensional drag coefficient (1.4×10^{-3}), u and v are the zonal and the meridional components of the geostrophic wind, respectively, ρ_{sw} is the average density of seawater ($\approx 1025\ \mathrm{kg\ m^{-3}}$), and $f = 2\Omega \sin(\theta)$ is the Coriolis parameter (Ω is the angular velocity of the Earth and θ the latitude)). The zonal and meridional components of the geostrophic wind were computed as follows:

$$u = \frac{-\alpha}{f}\frac{\partial p}{\partial y} \text{ and } v = \frac{\alpha}{f}\frac{\partial p}{\partial x}$$

where $\alpha = 1/\rho_a$. A friction correction (30% wind speed reduction and 15° wind direction shift) was applied by the IEO to these geostrophic winds before the upwelling estimate is computed (Bakun, 1973; Lavín et al., 1991). The UI was multiplied by a factor of 1000, so that the measure translates a displacement of volume for each kilometer of coast ($\mathrm{m^3\ s^{-1}\ km^{-1}}$).

UI is positive when the Ekman transport is oriented offshore (i.e. westward) and thus upwelling-favorable, and negative when the Ekman transport is onshore (eastward) and thus downwelling-favorable.

The six locations (a–f) at which the UI was computed and analyzed in this study are shown in Fig. 1. Throughout the analysis we used monthly-averaged UI indices computed from the 6-hourly data available at the IEO database.

In addition, for validation purposes (see Section 3.1), we have also used real wind measurements from a buoy located near Cabo Silleiro (9.43°W, 42.12°N) also provided by the Spanish Institute of Oceanography. Wind components from the Silleiro buoy (u and v) are available at a 6-hourly basis since 1999. In this case the UI was computed directly from the meridional wind stress using the real wind components measured at the buoy, which was also monthly-averaged from the 6-hourly data.

2.2. Circulation weather types

The classification used herein is an automated version of the Lamb weather type procedure, initially developed for the United Kingdom (Jones et al., 1993), and often named circulation weather types (CWTs). As mentioned before, this method has successfully been applied in other studies in western Iberian Peninsula, namely on precipitation trends and variability (Trigo and DaCamara, 2000) or lightning activity (Ramos et al., 2011).

Using an algorithm previously developed by Trigo and DaCamara (2000), we computed the daily CWTs for the 1967–2011 period by means of the daily sea level pressure (SLP) on a 2.5° latitude–longitude grid retrieved from the NCEP/NCAR reanalysis data (Kistler et al., 2001).

The circulation conditions were determined using the geostrophic wind approximation and adopting physical or geometrical parameters, such as the direction and strength of airflow and degree of cyclonicity. The indices used were the following: southerly flow (SF), westerly flow (WF), total flow (F), southerly shear vorticity (ZS), westerly shear vorticity (ZW), and total shear vorticity (Z). All these indices were computed using SLP values obtained for the 16 grid points (p1–p16), as shown in Fig. 1. Following the results obtained by Trigo and DaCamara (2000) we used the following expressions when computing the indices:

$$\mathrm{SF} = 1.305[0.25(\mathrm{p5}+2\mathrm{p9}+\mathrm{p13}) - 0.25(\mathrm{p4}+2\mathrm{p8}+\mathrm{p12})]$$
$$\mathrm{WF} = [0.5(\mathrm{p12}+\mathrm{p13}) - 0.5(\mathrm{p4}+\mathrm{p5})]$$
$$\mathrm{ZS} = 0.85[0.25(\mathrm{p6}+2\mathrm{p10}+\mathrm{p14}) - 0.25(\mathrm{p5}+2\mathrm{p9}+\mathrm{p13}) - 0.25(\mathrm{p4}+2\mathrm{p8}+\mathrm{p12}) + 0.25(\mathrm{p3}+2\mathrm{p7}+\mathrm{p11})]$$
$$\mathrm{ZW} = 1.12[0.5(\mathrm{p15}+\mathrm{p16}) - 0.5(\mathrm{p8}+\mathrm{p9})] - 0.91[0.5(\mathrm{p8}+\mathrm{p9}) - 0.5(\mathrm{p1}+\mathrm{p2})]$$
$$F = (\mathrm{SF2}+\mathrm{WF2})1/2$$
$$Z = \mathrm{ZS}+\mathrm{ZW}$$

The conditions established to define different types of circulation are the same as by Trigo and DaCamara (2000), and the following set of rules was applied:

(1) Direction of flow was given by $\tan^{-1}$(WF/SF), 180° being added if WF was positive. The appropriate direction was computed using an eight-point compass, allowing 45° per sector.
(2) If $|Z| < F$, the flow is essentially straight and was considered to be of a pure directional type (eight different cases, according to the directions of the compass).
(3) If $|Z| > 2F$, the pattern was considered to be of a pure cyclonic type if $Z > 0$, or of a pure anticyclonic type if $Z < 0$.
(4) If $F < |Z| < 2F$, the flow was considered to be of a hybrid type and was therefore characterized by both direction and circulation (8×2 different types).

These rules allow identifying 26 different types of weather circulation types or classes. In order to work out a more practical, though reliable, statistical analysis scheme for the frequency analysis, the 26 circulation types (10 pure, eight anticyclonic hybrids and eight cyclonic hybrids) were re-grouped into 10 basic ones. To do so, we adopted a similar procedure to that of Jones et al. (1993) and Trigo and DaCamara (2000): each of the 16 hybrid types was included with a weight of 0.5 into the corresponding pure directional and cyclonic/anticyclonic type frequencies (e.g. one case hybrid like the A.NE is included as 0.5 in A and 0.5 in NE). Therefore, we obtain 10 circulation types, eight driven by the direction of the wind flow (NE, E, SE, S, SW, W, NW, and N) and two by the shear vorticity (cyclonic or anticyclonic). Thus, 10 distinct CWTs are considered, including eight directional types dominated by strong non-rotational flow (within 45° sectors), and two other CWTs dominated by high absolute values of geostrophic vorticity (cyclonic and anticyclonic types).

We would like to stress that two distinct atmospheric SLP fields were used here to compute the UI and CWTs, and that these were originally derived from independent sources. As mentioned before, the UI was computed from the 6-hourly, 1° grid box SLP fields obtained from the U.S. Navy Fleet Numerical Meteorology and Oceanography Center (FNMO) distributed by the Pacific Fisheries Environmental Laboratory (PFEL), while the CWTs were computed from the 2.5° grid box SLP fields of the NCEP/NCAR reanalysis.

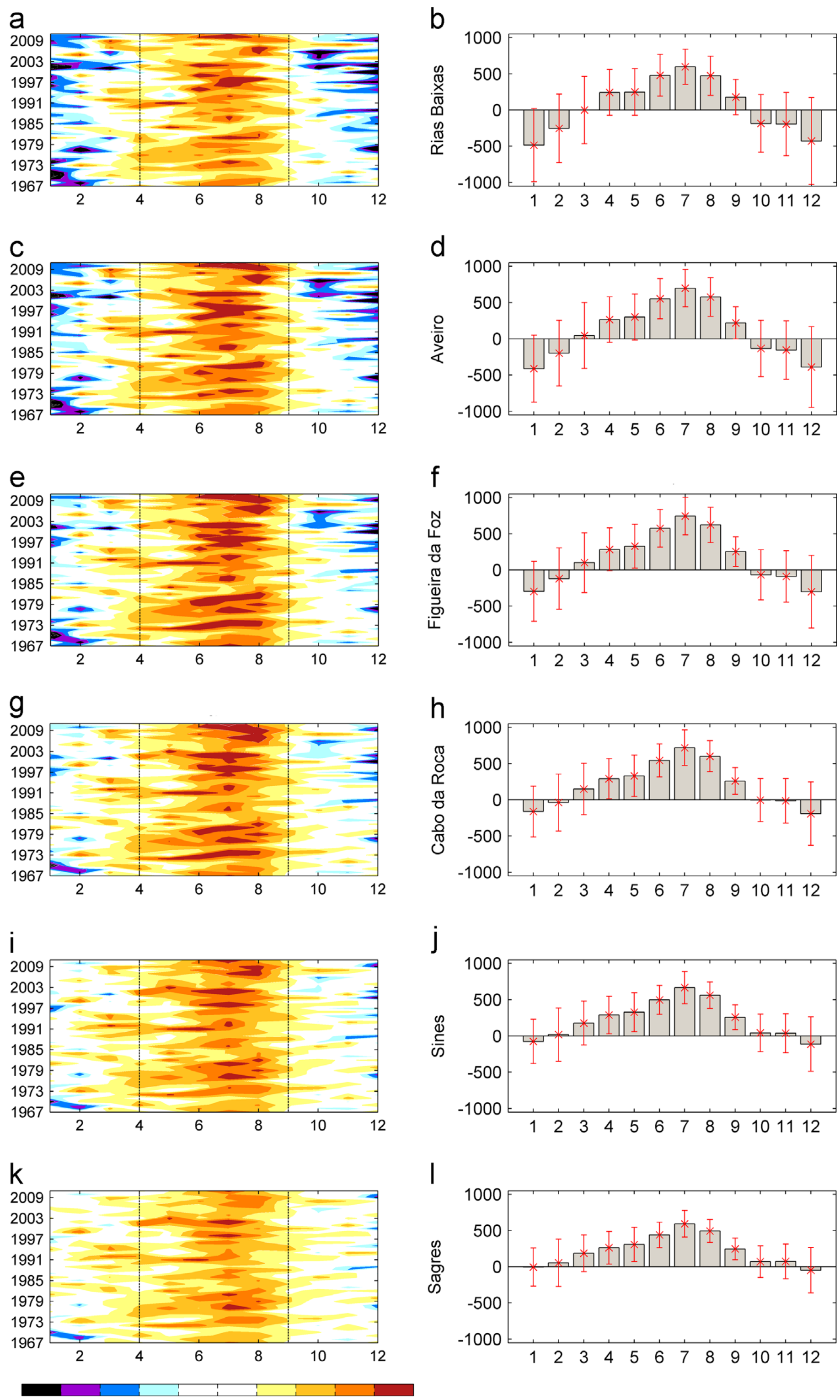

Fig. 2. Hovmöller diagrams of the monthly-averaged UI ($m^3\ s^{-1}\ km^{-1}$) (left column) and monthly distribution of UI intensity ($m^3\ s^{-1}\ km^{-1}$) with associated errors (right column) for Rias Baixas (a) and (b); Aveiro (c) and (d); Figueira da Foz (e) and (f); Cabo da Roca (g) and (h); Sines (i) and (j); and Sagres (k) and (l).

2.3. Statistical modeling of the UI

In order to reproduce monthly UI series, a forward stepwise regression was applied, using CWTs monthly frequencies as a pool of possible predictors (details and results in Sections 3.3 and 3.4). We have only considered, as eligible predictors, the ones presenting an absolute value of the Pearson correlation coefficient with the observed UI series above 0.4. A level of statistical significance of 5% was chosen in the stepwise regression method for predictor rejection, and the model was forced to retain at most four predictors. A stringent cross-validation scheme ("leave-one-out scheme") was applied with many distinct calibration and validation periods, as this tool enables a more robust procedure of selection–rejection. Additionally, it is also used in order to avoid over-fitting (Wilks, 2006), thus implying that the hindcast for each particular year was obtained from a model based on the remaining 44 year data.

UI monthly anomalies for the different locations were calculated against the 1967–2011 mean UI values of the April–September period altogether, in order to be used as predictands in individual models for each specific location. This procedure produces anomaly series with 270 timesteps, a much longer sample than the shorter series (45 timesteps), which would mean developing one individual model for each specific month (thus reducing once again the danger of over-fitting). The resultant predicted monthly anomaly series where afterwards converted into absolute monthly UI values using the April–September mean.

In order to check model performance, we will present the explained variance (R^2), the mean absolute error (MAE), and the skill score against the climatology (SS), being the latter given by

$$SS = \frac{RMSE - RMSEref}{RMSEperf - RMSEref} \times 100\%,$$

where the *RMSEref* is the root mean square error of the climatology series, and a perfect model would have *RMSEperf* equal to 0.

3. Results and discussion

3.1. Upwelling index

The UI mean seasonal and interannual distribution for each location is shown in Fig. 2. It is evident that the strongest upwelling signal takes place between April and September, i.e. corresponding to the late spring/summer months, as expected from the well-known behavior of mid-latitude upwelling systems, and in particularly the Iberian Upwelling System (Wooster et al., 1976; Fiúza, 1983). Also noteworthy is the similarity between locations of the UI patterns given by the Hovmöller diagrams (left column), although they vary in magnitude. In general, years with early upwelling onset are followed by years with late upwelling onset, seen by the left-to-right slope of the contours in the diagrams. There are some years that register favorable upwelling conditions during winter (February–March), and these are usually the years where the upwelling season lingers on until October (1973, 1983, 1992, 2000, to name a few). For instance, 2007 was a year with a particularly long upwelling season, which lasted from mid-February to mid-November; however, UI rarely surpassed the magnitudes that characterize strong upwelling events (>600 $m^3\,s^{-1}\,km^{-1}$). This happens in general for the years of long upwelling seasons, such as the ones mentioned before. Curiously, strong El Niño Southern Oscillation (ENSO) positive events have been registered in the preceding years (1972, 1982 and 1991, according to the Climate Prediction Center of NOAA). ENSO has been known to influence the NW African upwelling region, where warm ENSO events lead to weaker northerly winds and therefore weaker upwelling (Roy and Reason, 2001).

As for years of strong downwelling conditions in winter, one can note the periods 1967–72 and 1977–78, year 1997, and the period 2001–2005. Pérez et al. (2010) also registered low annual mean UI values for these periods in the Rias Baixas location, especially the latter, which corresponds to a negative summer NAO. When comparing the summer SLP field with that of period 1973–75 (positive summer NAO), these authors found that north of 40°N there is a decrease of the SLP cross-shore gradient, giving rise to a shift in the geostrophic wind from northerlies to westerlies, that is, changing from upwelling-favorable to downwelling-favorable conditions.

This analysis is reinforced by the seasonal average intensity per region and associated error bars (which were computed taking into account monthly UI values) displayed in Fig. 2, right column. Once again, this seasonal cycle is in agreement with previous studies on the characterization of upwelling seasonality for the western Iberian region (e.g. Wooster et al., 1976; Gómez-Gesteira et al., 2008). In general, UI is positive from March to September, being strongest in July, and negative from November to February, being strongest in January. Error bars are larger during winter months, decreasing in summer months, which implies that while in summer (JJA) conditions are always favorable for upwelling, in winter (as well as some of the transient months) some years are upwelling-favorable and others downwelling-favorable, although the latter prevail. Rias Baixas (Fig. 2b) presents the lowest positive UI in summer and the highest downwelling conditions in winter. This can be accounted for by the special characteristics of NW Iberian Peninsula (Torres et al., 2003), where the wind seasonality is more variable than on more southern locations, and the jagged estuaries and closed embayments make the coastline less linear. As we move southward, upwelling-favorable conditions intensify and downwelling-favorable weaken. However, it should be noted that the associated errors vary on the opposite direction, i.e. they tend to decrease when we move southwards. In the southernmost location downwelling conditions in winter are almost non-existing and positive UI during summer decreases, with values more similar to the northern locations. From this figure we draw that the preferential period for favorable upwelling conditions is April–September (AMJJAS), as previously described in the literature (e.g. Fiúza, 1983). Therefore, from this point on, results will be analyzed for these months only.

The interannual evolution of the mean summer (April–September) UI since 1967 as a function of latitude is shown on Fig. 3. Note that, despite the strong variability present, the color scale is

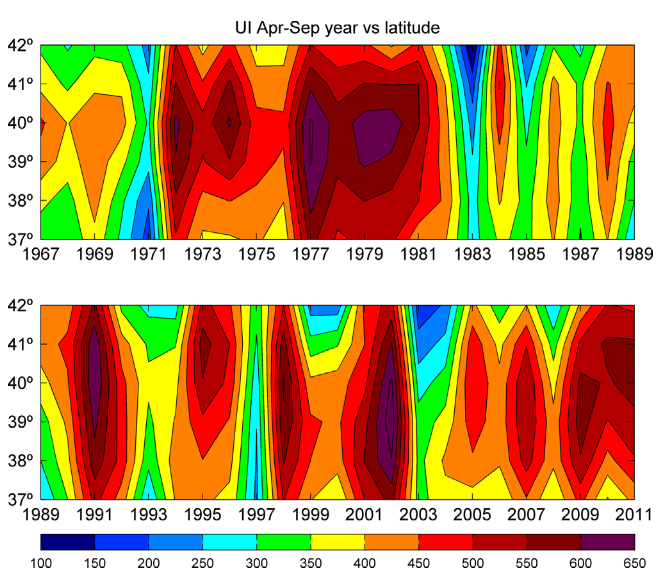

Fig. 3. Hovmöller diagram of summer averaged UI ($m^3\,s^{-1}\,km^{-1}$) (April–September) as a function of latitude.

always positive, that is, it is always upwelling-favorable conditions. From this diagram it is evident that UI has strong inter-annual variability. The UI signal is highly consistent for each year within the latitudinal range. That is, whether UI is high or low, the same is observed at all latitudes. Maximum values are in general observed between 39°N and 40°N. A possible explanation for higher UI values at these latitudes is that the upwelling-associated filaments generated from the equatorward advection of the cold and fresh upwelled waters are sometimes enhanced by the topographic feature of the Estremadura Promontory and can thus have a jet-like nature (Haynes et al., 1993; Oliveira et al., 2009). There are 5 years where upwelling occurrence is particularly strong: 1977, 1979, 1991, 1998 and 2002. The 1991 maximum may be related to the early 1990s winter NAO maximum (Santos et al., 2005), which these authors found to be a turning point towards a period of stronger upwelling occurrence, although such strengthening is not evident in our results. Peliz et al. (2002) report that in August 1998 western Iberian Peninsula was under constant northerly winds for practically the entire month, likely accounting for the strong signal of that year. On the other hand, there are also 5 years where upwelling episodes are visibly weak, namely: 1971, 1983, 1985, 1997 and 2003. Nykjaer and Van Camp (1994) reported a weak upwelling period in the Canary Upwelling System in 1983–84 due to an exceptional strong El Niño Southern Oscillation (ENSO) in the Pacific Ocean in the previous year. Furthermore, some of these years show rather an increase of UI with increasing latitude instead of maxima at 39/40°N (e.g. 1983, 1985, 1999, and 2003).

Before going any further, in order to validate the UI index presented in the work we used additional wind buoy data to compare it with the UI computed from the FNMOC SLP fields. This comparison was made between the study location of Rias Baixas (10°W, 42°N, Fig. 1, location a) and the nearest buoy, which is located near Cabo Silleiro (9.43°W, 42.12°N), since 1999. The approximate distance between the two locations is 50 km.

Monthly correlation values (April–September) between the two time series of the UI (Rias Baixas and Cabo Silleiro) were computed and results show that the time series are significantly correlated (at the 5% level) in all months, except in July. In addition, the correlation between the annual AMJJAS average is 0.588 (significant at the 5% level). These results are similar in magnitude to those found by previous authors that have performed a similar analysis for this region (Cabanas and Alvarez, 2005). According to these authors, the accuracy of historical UI

Table 1
Pearson correlation coefficient between the monthly UI index and the monthly frequencies of each subtype of the Lamb classification, for the period 1967–2011.

	NE	E	SE	S	SW	W	NW	N	C	A
Rias Baixas										
April	<u>0.56</u>	<u>0.42</u>	−0.23	−0.21	−<u>0.66</u>	−<u>0.59</u>	−0.22	<u>0.44</u>	−0.03	−0.05
May	<u>0.72</u>	<u>0.33</u>	−0.14	0.25	−<u>0.59</u>	−<u>0.59</u>	−0.16	<u>0.55</u>	−<u>0.32</u>	−0.19
June	<u>0.61</u>	0.07	−0.05	−0.23	−<u>0.60</u>	−<u>0.57</u>	−0.16	0.16	−0.10	−0.19
July	<u>0.62</u>	0.27	−0.13	0.09	−0.22	−<u>0.44</u>	−<u>0.52</u>	0.19	−0.27	−<u>0.36</u>
August	<u>0.77</u>	0.29	−0.06	0.08	−<u>0.48</u>	−<u>0.59</u>	−<u>0.34</u>	0.15	−0.11	−<u>0.45</u>
September	<u>0.78</u>	0.27	−0.13	0.03	−<u>0.56</u>	−<u>0.53</u>	−0.28	0.03	−0.04	−0.24
Aveiro										
April	<u>0.54</u>	<u>0.30</u>	−<u>0.30</u>	−<u>0.30</u>	−<u>0.67</u>	−<u>0.52</u>	−0.18	<u>0.48</u>	−0.14	0.08
May	<u>0.67</u>	0.23	−0.16	0.23	−<u>0.60</u>	−<u>0.54</u>	−0.15	<u>0.59</u>	−<u>0.40</u>	−0.08
June	<u>0.51</u>	0.06	−0.06	−0.22	−<u>0.60</u>	−<u>0.57</u>	−0.15	0.24	−0.17	−0.12
July	<u>0.53</u>	0.16	−0.11	−0.04	−0.22	−<u>0.38</u>	−<u>0.50</u>	0.24	−<u>0.38</u>	−0.22
August	<u>0.76</u>	0.20	−0.03	0.06	−<u>0.44</u>	−<u>0.58</u>	−<u>0.33</u>	0.19	−0.18	−<u>0.41</u>
September	<u>0.64</u>	0.14	−0.23	−0.04	−<u>0.62</u>	−<u>0.40</u>	−0.26	0.17	−0.26	−0.02
Figueira da Foz										
April	<u>0.53</u>	0.19	−<u>0.38</u>	−<u>0.33</u>	−<u>0.65</u>	−<u>0.43</u>	−0.12	<u>0.51</u>	−0.24	0.17
May	<u>0.60</u>	0.10	−0.16	0.15	−<u>0.58</u>	−<u>0.47</u>	−0.13	<u>0.62</u>	−<u>0.48</u>	0.02
June	<u>0.44</u>	0.02	−0.08	−0.22	−<u>0.57</u>	−<u>0.56</u>	−0.16	0.29	−0.29	−0.01
July	<u>0.40</u>	0.08	−0.09	−0.07	−0.25	−<u>0.33</u>	−<u>0.45</u>	<u>0.30</u>	−<u>0.45</u>	−0.07
August	<u>0.68</u>	0.07	−0.02	0.02	−<u>0.41</u>	−<u>0.54</u>	−0.25	0.24	−0.28	−<u>0.32</u>
September	<u>0.50</u>	0.03	−<u>0.33</u>	−0.12	−<u>0.63</u>	−0.23	−0.22	0.27	−<u>0.42</u>	0.16
Cabo da Roca										
April	<u>0.51</u>	0.06	−<u>0.44</u>	−<u>0.36</u>	−<u>0.61</u>	−<u>0.33</u>	−0.08	<u>0.51</u>	−<u>0.32</u>	0.24
May	<u>0.54</u>	−0.01	−0.16	0.09	−<u>0.54</u>	−<u>0.41</u>	−0.12	<u>0.64</u>	−<u>0.53</u>	0.12
June	<u>0.34</u>	0.00	−0.09	−0.23	−<u>0.52</u>	−<u>0.52</u>	−0.16	<u>0.30</u>	−<u>0.40</u>	0.14
July	0.25	0.00	−0.04	−0.13	−0.28	−<u>0.30</u>	−<u>0.38</u>	<u>0.37</u>	−<u>0.50</u>	0.06
August	<u>0.56</u>	−0.05	−0.01	−0.03	−<u>0.36</u>	−<u>0.46</u>	−0.14	0.24	−<u>0.37</u>	−0.19
September	<u>0.39</u>	−0.09	−<u>0.43</u>	−0.19	−<u>0.61</u>	−0.11	−0.17	0.32	−<u>0.50</u>	0.27
Sines										
April	<u>0.48</u>	−0.01	−<u>0.48</u>	−<u>0.38</u>	−<u>0.54</u>	−0.25	−0.06	<u>0.51</u>	−<u>0.37</u>	0.28
May	<u>0.50</u>	−0.06	−0.15	0.08	−<u>0.51</u>	−<u>0.36</u>	−0.14	<u>0.61</u>	−<u>0.56</u>	0.17
June	0.22	0.02	−0.10	−0.21	−<u>0.47</u>	−<u>0.46</u>	−0.15	0.28	−<u>0.47</u>	0.27
July	0.15	−0.03	0.01	−0.19	−0.29	−0.28	−<u>0.32</u>	<u>0.39</u>	−<u>0.51</u>	0.15
August	<u>0.44</u>	−0.14	0.03	−0.06	−0.29	−<u>0.37</u>	−0.07	0.24	−<u>0.44</u>	−0.08
September	<u>0.34</u>	−0.18	−<u>0.50</u>	−0.23	−<u>0.59</u>	−0.04	−0.15	<u>0.32</u>	−<u>0.53</u>	<u>0.36</u>
Sagres										
April	<u>0.45</u>	−0.05	−<u>0.51</u>	−<u>0.37</u>	−<u>0.48</u>	−0.20	−0.07	<u>0.48</u>	−<u>0.43</u>	<u>0.33</u>
May	<u>0.46</u>	−0.09	−0.15	0.05	−<u>0.46</u>	−<u>0.30</u>	−0.18	<u>0.60</u>	−<u>0.62</u>	0.25
June	0.11	0.03	−0.12	−0.15	−<u>0.40</u>	−<u>0.41</u>	−0.15	0.26	−<u>0.51</u>	<u>0.38</u>
July	0.11	−0.08	0.02	−0.22	−<u>0.31</u>	−0.28	−0.26	<u>0.37</u>	−<u>0.54</u>	0.24
August	<u>0.32</u>	−0.23	0.09	−0.07	−0.24	−<u>0.36</u>	0.01	0.23	−<u>0.52</u>	0.07
September	0.23	−0.25	−<u>0.54</u>	−0.27	−<u>0.54</u>	0.04	−0.09	<u>0.31</u>	−<u>0.56</u>	<u>0.44</u>

Underlined values are statistically significant at the 5% level.

series (located at 11°W, 43°N), computed from large scale sea level pressure charts provided by the Spanish met office, is checked by comparing the UI series obtained from different sources, including (their Table 1): (a) SLP fields obtained from the FNMOC dataset; (b) SLP fields derived from a mesoscale meteorological model provided by Meteogalicia (the Galician official met office); and (c) wind data obtained from the SeaWind microwave radar on board of the NASA's Quick Scatterometer (QuikSCAT).

Although originating from different sources/methods, (b) and (c) series can be considered mesoscale series, while (a) and historical UI series correspond to synoptic scale. It was shown also by Cabanas and Alvarez (2005) that the correlation between these two synoptic scale indices is close to 1. On the other hand, when comparing UI historical series against the data from either the mesoscale model or QuikSCAT the correlation decreases to values near 0.6 (but still statistically significant at the 5% level), which is in fact the magnitude of values that we found when comparing synoptic scale (UI based on a large-scale mode—SLP fields) against mesoscale (UI based on real measured wind at the buoy).

3.2. Circulation weather types

The daily CWTs for the entire 45-years-long period (1967–2011) were computed using the same methodology as Trigo and DaCamara (2000) (see Section 2.2).

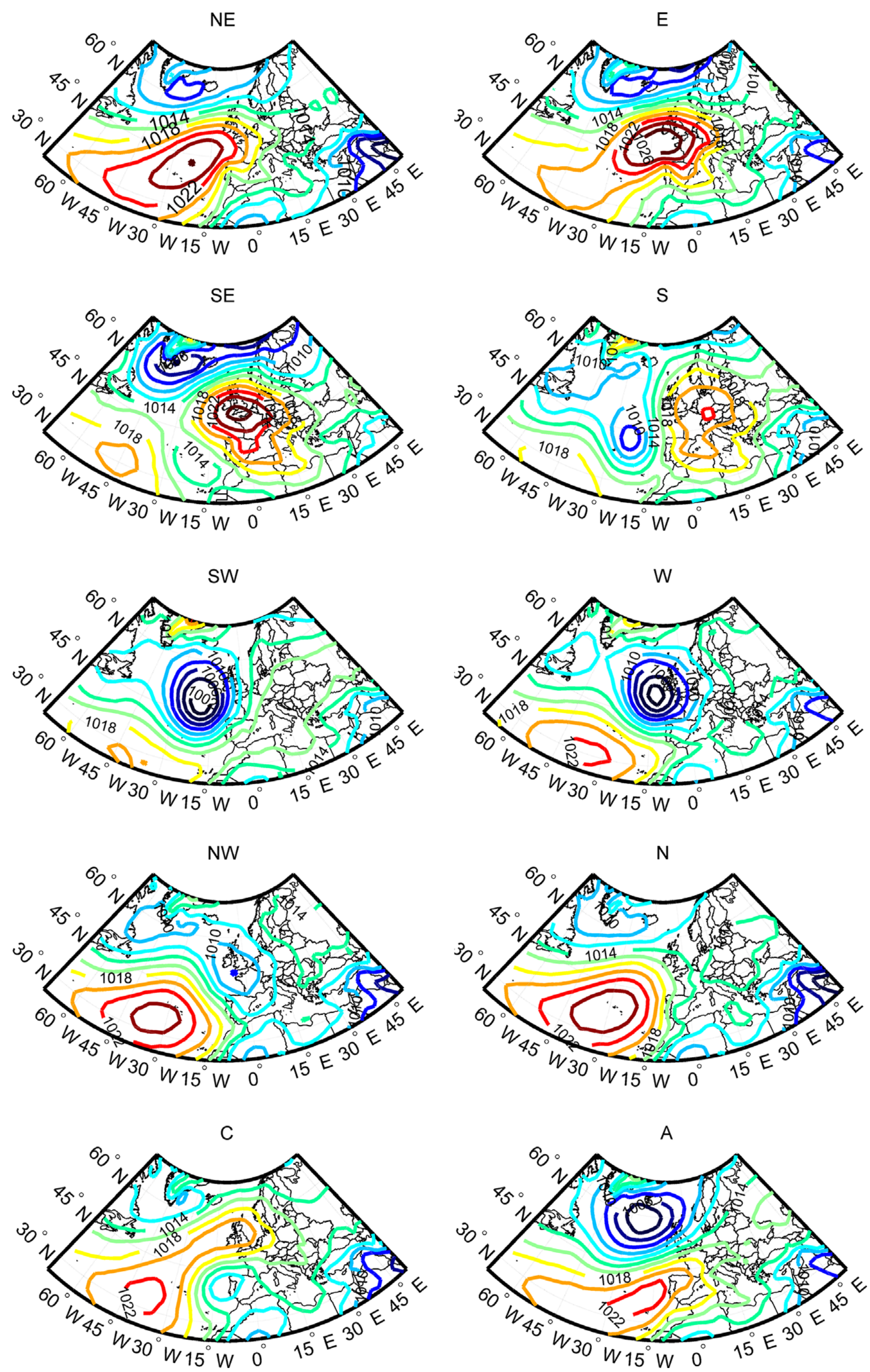

Fig. 4. Composite map computed for April–September, of the SLP fields for the eight directional weather types and two vorticity weather types. These composites were computed using the NCEP/NCAR reanalysis for the 1967–2011 period.

Since the months with the highest values of UI were identified to span from April to September, the CWTs analysis will only focus on these months. The composites of SLP for the 1967–2011 period and for AMJJAS months for the 10 CWTs retained are shown in Fig. 4. In the directional CWTs (NE, E, SE, S, SW, W, NW and N) the conditions of the wind direction correspond to the respective weather type name. That is, the NE type corresponds to days with NE wind conditions in the center of the domain where the CWTs are computed, and so on. A short description of each type is given here:

- NE (north-easterly) days are characterized by an extended Azores high (pressure) towards the British Islands and by low-pressure values of SLP over the Mediterranean region;
- E (easterly) days correspond to synoptic situations characterized by an anticyclone centered east off the British Isles;
- SE (south-easterly) days are characterized by low-pressure regions extending from Madeira to the east of the Azores Islands centered in the British Isles;
- S (southerly) represents situations characterized, on average, by a high-pressure system located over central Europe;
- SW (south-westerly) days are characterized by a weakening of the Azores high (pressure) and strong low pressure located between Iceland and the Azores;
- W (westerly) days are characterized by the setting of the Azores high (pressure) around 30°N and by the presence of deep low-pressure centers west of France;
- NW (north-westerly) days are characterized by a southward displacement of the usual location of Azores high (pressure) and a low-pressure centered off northern France;
- N (northerly) days are characterized by the presence of the Azores high-pressure center over the Azores Islands and low SLP values over the Mediterranean basin;
- C (cyclonic) days correspond to relatively strong low-pressure systems located close or over the western Portuguese coast, sometimes accompanied by a blocking anticyclone located over the British Isles. The wind direction depends on the position of the low-pressure, and changes during the crossing of the systems, but on the overall, westerly winds tend to dominate as we progress towards southern Portugal. These days are often characterized by strong winds; and
- A (anticyclonic) days are characterized by an extended high-pressure center between the Iberian Peninsula and the Azores Islands. Conditions along the western Iberian Peninsula coast are generally characterized by SW winds in northwestern Iberia, while SE winds can be found in the southern Portuguese coast. Nevertheless, this type is generally characterized by lighter winds, resulting from smaller pressure gradients associated with the close position of the high-pressure system.

The April–September mean frequency (in %) for the 10 CWTs for the 1967–2011 period is shown in Fig. 5. The NE type (near 23%) and the N type (around 17%) along with the A type (25%) are the most frequent CWTs during the analyzed period, with these three types being responsible for almost 70% of the total number of days analyzed. The cyclonic type is responsible for 10% of the total number of days. On the contrary, the southerly types (SW, S and SE) along with the E type are the least frequent CWTs, occurring during less than 12% of the totality of considered days.

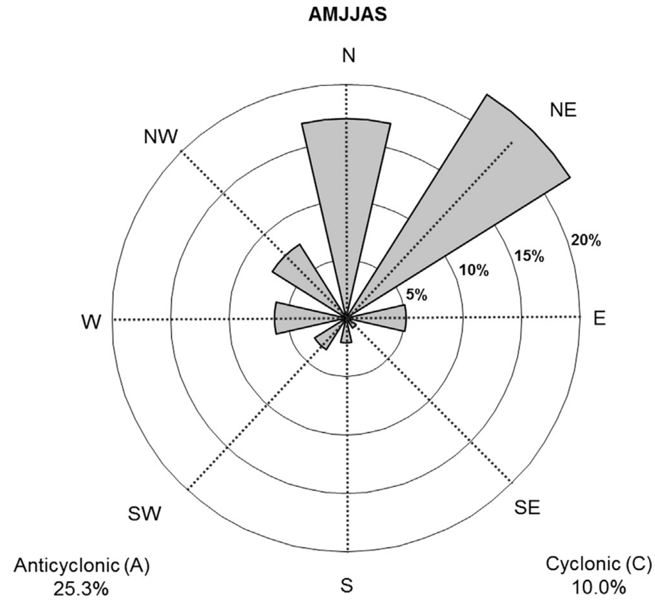

Fig. 5. Mean circulation weather types frequencies (%) during the April–September months. These frequencies were computed using the NCEP/NCAR reanalysis SLP fields for the 1967–2011 period.

3.3. *Relationship between the upwelling index and circulation weather types*

CWTs can provide a simple characterization of synoptic weather variability, and this variability is bound to exert a major effect over upwelling episodes on the study area (e.g. deCastro et al., 2008). Although coastal upwelling may be acknowledged at sub-synoptic scales, the forcing mechanisms that foster strong and generalized upwelling events in the western coast of Iberian Peninsula are highly related to sea level pressure configurations that promote wind fluxes from the northerly quadrant. Furthermore, it is well known that these situations are usually associated to stable conditions, with such wind fluxes being forced by the location of high pressure systems in the Atlantic sector (deCastro et al., 2011). At this spatial scale, CWTs are quite capable of reproducing the variability of pressure fields, both for the daily time-scale as well as for intra-annual variability (e.g. Ramos et al., 2010).

Bearing this in mind, the objective in this section is to analyze to what extent is upwelling variability associated with just a few CWTs. For this purpose, we computed the Pearson correlation coefficients between monthly frequencies of CWTs and corresponding UI monthly series. In order to avoid the inflation of correlation coefficients (as a consequence of trends in the series), the existence of statistical trends in the time series was tested with a more elaborated version of the Mann–Kendall test (Hamed and Ramachandra, 1997) that takes into account the autocorrelation of the series (Sousa et al., 2011). This procedure was applied to the UI series of all six considered sites and no significant trends were found (at the 5% level).

The results for the correlation analysis (during the April–September period) are summarized in Table 1, being relatively similar for all six sites. Taking into account the roughly north–south orientation of the coastline higher UI values are expected to take place with wind fluxes from a northerly quadrant. A synoptic flow from this quadrant may also be accentuated by the breeze circulation, which also flows from a northerly direction in western Iberian Peninsula coastal areas. However, it is very important to notice that the considered CWTs patterns are directly related with geostrophic flow, not real flow. The latter is in fact oriented several degrees towards lower pressure systems (counterclockwise in the Northern Hemisphere) due to the effect of surface friction (Wallace and Hobbs, 2006). This fact explains why the NW type does not show significant links with UI, as in fact this pattern is more related with WNW winds that do not favor upwelling; rather it can even promote some downwelling. On the other hand, this slight bias in real wind direction versus weather type direction explains why the NE type presents the highest correlation

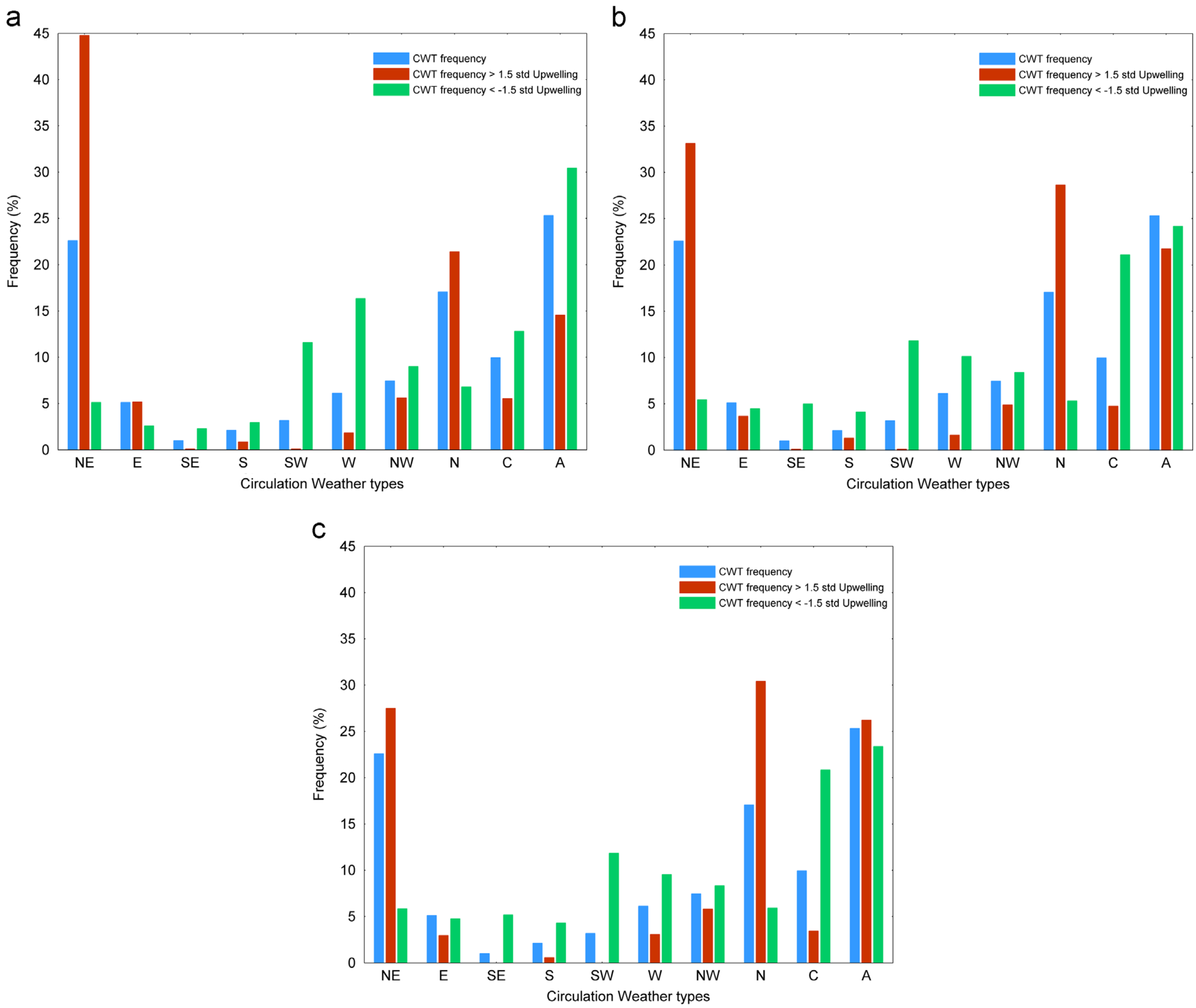

Fig. 6. Circulation weather types averaged frequencies under three different UI conditions for three selected locations: (a) Rias Baixas, (b) Cabo da Roca and (c) Sagres. Results are shown for the April–September period of analysis (blue), the months with the most favorable conditions for upwelling (i.e. UI values above 1.5 std, red) and the months with the least favorable conditions for upwelling (i.e. UI values below −1.5 std, green). (For interpretation of the references to color in this figure legend, the reader is referred to the web version of this article.)

coefficients with UI. It is the weather type that is responsible for the most alongshore winds (essentially north–south). The NE type presents correlations above 0.5 for almost all months and locations, reaching even values above 0.7 for the two northernmost stations (Rias Baixas and Aveiro). The second CWT most related to UI is the N type, also with correlation coefficients frequently above 0.5, especially in southern locations. The E type is also related with offshore flow and the occurrence of upwelling, but correlation coefficients for this type are relatively low, as this type of synoptic conditions generally does not originate very intense winds, when compared to northerly fluxes, where the synoptic flow is emphasized by the breeze circulation. On the other hand, significant anti-correlation values are also found with a few CWTs, implying important links between certain CWTs and non-favorable upwelling conditions. Anti-correlation values stronger than −0.5 are found for the W and SW types in almost all locations, with the exception for the W type in Sines and Sagres, where correlation values never fall below −0.5. Naturally, these types tend to originate onshore winds, which promote downwelling. In southern locations (Sagres, Sines and Cabo da Roca) the C type is also highly correlated with non-favorable upwelling conditions (below −0.5). Other types have some reasonable links in some months, but do not always present a coherent (and statistically significant) signal throughout the summer months. This is easily understandable, as they are related with marginal wind fluxes in terms of direction when compared to the two previous extreme cases.

To further investigate the relationship between CWTs and UI we have searched for the months with the most and the least favorable conditions for upwelling (between April and September). Months with intense upwelling activity are identified as those where UI values were at least 1.5 standard deviations above the AMJJAS mean for the entire 1967–2011 period. On the contrary, months with less pronounced upwelling activity are identified as those months where UI values were at least 1.5 standard deviations below the AMJJAS mean for the entire 1967–2011 period. For this analysis, we selected three out of the six locations for the sake of simplicity: Rias Baixas and Sagres, the northernmost and southernmost location, respectively, and also an intermediate site, Cabo da Roca. We could just as well have chosen Figueira da Foz as representative of a midway location along Western Iberian Peninsula; however we opted for Cabo da Roca considering the occurrence of stronger upwelling events in that sector (Fig. 3). For the selected locations presented later in Figs. 6 and 7 (Rias Baixas, Cabo da Roca and Sagres) the corresponding means (standard deviations) mentioned above are respectively: 370.5 (319.9) $m^3 s^{-1} km^{-1}$, 457.4 (295.3) $m^3 s^{-1} km^{-1}$ and 389.7 (228.8) $m^3 s^{-1} km^{-1}$.

CWTs mean frequencies were computed for those two specific anomalous months (most and least favorable upwelling activity), and are shown in Fig. 6 for the three selected locations. In addition, results are also compared with the April–September mean frequencies (in %) of the CWTs relative to the 1967–2011 period (results already shown in Fig. 5). It was found that, in Rias Baixas (Fig. 6a) and Cabo da Roca (Fig. 6b), for months with more upwelling-favorable conditions, there is an important increase in April–September mean CWTs frequencies of the N and NE types along with a decrease in the other CWTs (more prominent in the A and C types). In Sagres (Fig. 6c), besides the increase of the N and NE types (as in the other two locations) there is also an increase of the A type.

Focusing on the anomalous months with less upwelling-favorable conditions, a pronounced decrease is found for N and NE types in all locations, while less significant decreases occuring for the E type in Rias Baixas (Fig. 6a) and Cabo da Roca (Fig. 6b) and for the A type in Sagres (Fig. 6c). Simultaneously, an increase in other types occurs, more pronounced for the SW, W and C types. These results are in agreement with the ones found in Table 1.

3.4. Statistical modeling of the upwelling index

The statistically significant links found between UI and the CWTs series raise the prospect of developing simple, yet hopefully robust, statistical models to reproduce the variability of the upwelling phenomenon in the western coast of the Iberian Peninsula. In the previous section, it has been shown that the N, NE and E types are, essentially, the CWTs better related with upwelling events in this area, while the W and SW types are linked with less upwelling-favorable conditions episodes. Bearing in mind that high monthly frequencies of these CWTs explain a large part of the variability of UI monthly means, we have applied a multi-linear regression model to hindcast UI monthly series. For this purpose, as explained in Section 2.3, a forward stepwise regression was applied, using the contemporary CWTs monthly frequencies as predictors, and applying a cross-validation scheme. The relevance of previous meteorological conditions was also checked, by analyzing links between the UI and the preceding months CWTs series. Results indicate a non-significant gain in model efficiency against the simpler model version, i.e. considering only CWTs without lag (not shown).

The UI series resulting from the hindcast models for the three chosen locations (Rias Baixas, Cabo da Roca and Sagres) are shown in Fig. 7, presenting continuous April–September data for the period of time spanning between 1967 and 2011. In Table 2 a summary of the statistics for model performance in all six locations is shown, including the Explained Variance (R^2), the Mean Absolute Error (MAE) and the Skill Score against climatology

Table 2
Model equations for the April–September UI series and corresponding explained variance (R^2), mean absolute error (MAE) and Skill Scores against the climatology (SS), for the period 1967–2011. All correspondent Pearson correlation coefficients (R) with the observed series are statistically significant at the 5% level.

Rias Baixas	UI = +10.8 NE + 5.8 N–18.4 SW–11.0 W + 370.4		
	SS = +78%	R^2 = 70%	MAE = 141 $m^3 s^{-1} km^{-1}$
Aveiro	UI = +10.6 NE + 8.8 N–20.1 SW–7.8 W + 434.8		
	SS = +77%	R^2 = 68%	MAE = 153 $m^3 s^{-1} km^{-1}$
Figueira da Foz	UI = +9.5 NE + 10.7 N–20.0 SW–4.5 W + 467.7		
	SS = +74%	R^2 = 63%	MAE = 156 $m^3 s^{-1} km^{-1}$
Cabo da Roca	UI = +5.8 NE + 9.3 N–18.8 SW–9.2 C + 457.4		
	SS = +76%	R^2 = 66%	MAE = 140 $m^3 s^{-1} km^{-1}$
Sines	UI = +4.8 NE + 8.8 N–17.2 SW–9.3 C + 432.8		
	SS = +66%	R^2 = 63%	MAE = 130 $m^3 s^{-1} km^{-1}$
Sagres	UI = +2.5 NE + 6.5 N–14.8 SW–9.0 C + 389.7		
	SS = +63%	R^2 = 61%	MAE = 115 $m^3 s^{-1} km^{-1}$

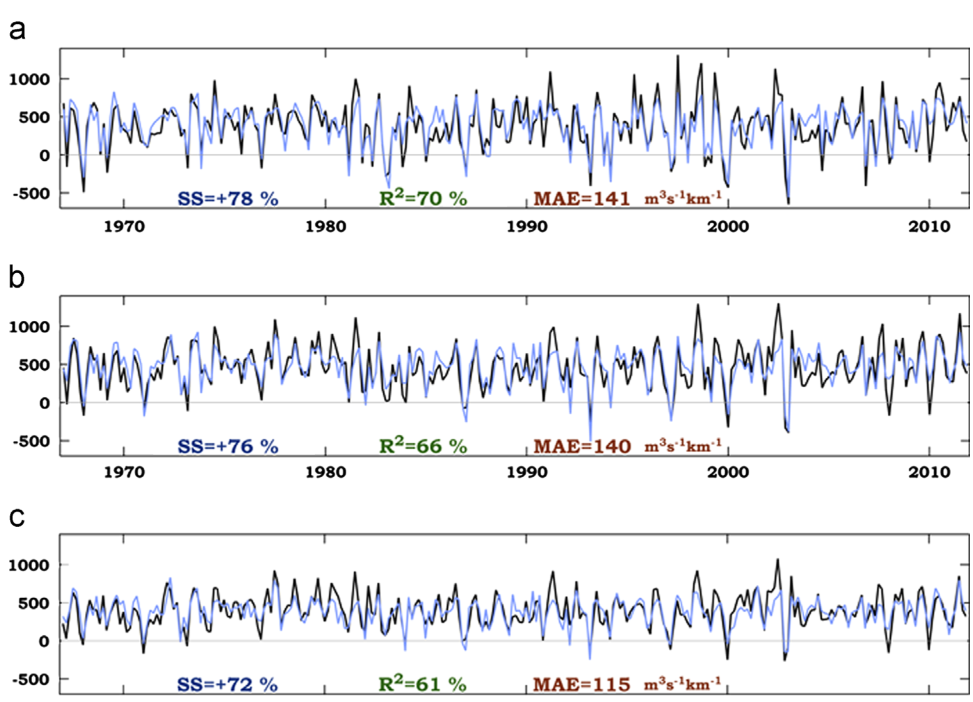

Fig. 7. Observed (black) and modeled (blue) UI monthly values (for the period April–September), and the correspondent Skill Score against climatology (SS), explained variance (R^2) and Mean Absolute Error (MAE), for three selected locations: (a) Rias Baixas, (b) Cabo da Roca and (c) Sagres. (For interpretation of the references to color in this figure legend, the reader is referred to the web version of this article.)

Table 3
Monthly explained variance (R^2) and mean absolute error (MAE) for the UI modeled series, for the period 1967–2011. All correspondent Pearson correlation coefficients (R) with the observed series are statistically significant at the 5% level.

	Rias baixas		Aveiro		Figueira da Foz		Cabo da Roca		Sines		Sagres	
	R^2	MAE	R^2	MAE	R^2	MAE	R^2	MAE	R^2	MAE	R^2	MAE
April	0.71	132	0.68	138	0.62	138	0.61	137	0.56	139	0.60	123
May	0.71	142	0.67	156	0.59	168	0.66	142	0.64	134	0.60	121
June	0.59	144	0.53	157	0.47	157	0.51	131	0.45	119	0.34	117
July	0.43	143	0.34	167	0.28	175	0.38	150	0.37	136	0.41	118
August	0.67	136	0.59	145	0.46	144	0.40	135	0.35	123	0.24	121
September	0.69	147	0.61	155	0.51	151	0.67	144	0.64	129	0.60	92

(SS). Model results were also aggregated by month in order to analyze monthly specificities of the UI variability—Table 3.

This relatively simple statistical modeling approach is capable of reproducing a large part of the variability of UI monthly series in all the considered regions, with high Skill Scores—above +70% (+60%) in the northernmost (southernmost) locations. High correlation coefficients are also obtained for the entire period, with correspondingly large fractions of explained variance (above 60%). In general, the model captures the timing of most peaks but with smaller amplitude than the observed series. However, the inability to reproduce some of the highest peaks in upwelling intensity appears to be the main caveat of the model. Looking in detail at the monthly scale (Table 3), the smallest values of SS and R^2 are found for July, as this appears to be the month where CWTs monthly frequencies explain the smallest fraction of the variance (Table 1). As stated before, this might be indicative that the mesoscale component of the upwelling processes is larger in mid-summer. This is a logical result given that July is the month with the largest mean land–sea temperature gradient, and therefore the peak in the climatology of thermal lows in the Iberian Peninsula (Hoinka and Castro, 2003), which are a driving process for land–sea breezes. This type of smaller scale processes is obviously not captured by the CWTs, and has a more significant impact in mid-summer upwelling than in other months, thus explaining these results.

The equations of the obtained models for UI monthly series in all the six locations are presented in Table 2, alongside with the respective SS, R^2 and MAE of each individual model. These equations do not present any unusual feature, since the chosen predictors correspond to the CWTs most closely linked to more favorable or less favorable upwelling conditions, as described in Section 3.3. In fact, the NE and N (promoting upwelling) types, as well as SW (promoting downwelling) are present in all six models, reinforcing the notion that the synoptic scale meteorological conditions that exert major control on upwelling occurrence are fairly similar all along the western coast of the Iberian Peninsula. On the overall, we can notice that there are two blocks of models, differing only in one of the predictors: W versus C—the first for the three northernmost locations, and the latter for the three southernmost locations. In fact, the W type is related to downwelling in all locations, but this result shows that it progressively loses impact in terms of promoting downwelling against cyclonic conditions as we move southwards.

4. Conclusions

In this work we studied the relationship between the variability on the occurrence of several circulation weather types and the variability of upwelling indices along the western coast of the Iberian Peninsula. An initial brief study of the intra- and interannual variability of upwelling index off western Iberian Peninsula was performed taking into account six locations (Rias Baixas, Aveiro, Figueira da Foz, Cabo da Roca, Sines and Sagres (Fig. 1)). The data is characterized by a strong seasonal cycle and a superimposed strong interannual variability, in agreement with previous works that have thoroughly described the Iberian Upwelling System (e.g. Relvas et al., 2007). UI is quite homogeneous along the western coast of the Iberian Peninsula; strong and weak upwelling signals in different years are observed at all latitudes, although with different intensities. Nevertheless, and since CWTs relationship with UI changes in latitude, we believed to be worthwhile establishing a complete portrait of the western Iberian Peninsula coast, and have therefore analyzed the relationship between circulation weather types and upwelling indices at those six different locations.

We had proposed ourselves to test if an automated version of the famous Lamb circulation weather types (originally developed for the UK) was capable of reproducing weather patterns that are linked with upwelling–downwelling events in western Iberian Peninsula. Focusing on the relationship between CWTs and UI, it is no surprise to find that northerly winds are highly correlated with upwelling events in these regions. In fact, this is even common sense, as these synoptic conditions are characterized and named by the local population as Nortada, well-known for cool water and rich fishery conditions (Fiúza, 1983). Further, this is also valid for downwelling episodes or, more accurately, weak upwelling episodes, with onshore (essentially W and SW types) or cyclonic conditions in terms of the circulation weather types.

The results obtained for the statistical models developed in this work are very satisfactory, since we were able to reconstruct with good accuracy a significant part of the explained variance (above 60%) of the observed UI time series, based solely on CWTs classification, and thus reproducing fairly well both seasonal and interannual variability of the UI. That is, we were able to characterize the upwelling conditions of the region at a synoptic scale. Results show that for all locations NE and N types are the main drivers for upwelling events, while the SW type dominates downwelling events. For northwestern (southwestern) locations, the W (C) type also drives downwelling episodes significantly. These results indicate that large-scale meteorological conditions (the essence of the considered circulation weather types) can explain the largest fraction of the variability of upwelling processes in the western coast of Iberia. However, as stated earlier, the authors are aware that mesoscale processes (namely land–sea breezes) also play a significant role in this variability. By analyzing the performance of the statistical models, it is clear that mesoscale processes are rather important in mid-summer, since this is the period where the circulation weather types-fed models present the worst results (particularly in July and August). During this time of the year, the relevance of both mesoscale and large-scale processes seems comparable, at least at the monthly time-scale, and probably the former are responsible for a large fraction of the remainder of explained variance not captured by the latter in the statistical models. The idea that this mid-summer period presents the most prominent episodes of mesoscale circulation induced upwelling events is further reinforced by the fact that July is usually the month with the highest frequency of thermal low patterns (Hoinka and Castro, 2003). The question of the role of mesoscale on upwelling systems has been addressed by previous authors such as Di Lorenzo et al. (2005) for the California Current System and by Relvas et al. (2009) for western Iberian Peninsula. The former found, for period 1949–2000, a warming trend attributed to surface heating and a strengthening of upwelling-favorable winds, which in turn increase current velocities and associated variance. This extra eddy activity, the authors postulate, may have implications in the decadal variability of the system. The latter, considering the different SST trends in the northern and southern coasts of Western Iberian Peninsula since 1985, attribute the differences to mesoscale activity associated with upwelling. This difference is higher for the core summer months (JJA).

Taking into consideration previous studies of interannual variability and upwelling trends, the data presented here does not show any clear increase or decrease of UI from 1967 to 2011 (Fig. 7). In terms of interannual variability, we have seen from Fig. 3 that the 70's (80's) were a decade of generally strong (weak) upwelling events, and that from 1990 on the intensity of UI alternates roughly every 2 years. Bakun (1990) observed similar behavior off Iberian Peninsula at 43°N, with general high UI in the 70's and oscillating UI in the 80's. Narayan et al. (2010), who have found both strengthening and weakening UI tendencies by analyzing several yearly-averaged UI time series, observed, for a similar period for a region off NW Africa, more accentuated UI variability after 1990.

We would like to stress out that the computing of the objective Lamb circulation weather types is a simple, yet a very cost-effective way to capture these atmospheric patterns. In addition, it can be easily adapted to other domains (both for Northern or Southern Hemisphere) and different gridded Sea Level Pressure datasets can be used in the computation of the CWTs. (e.g. NCEP/NCAR reanalysis (Ramos et al., 2011 and this work); EMULATE Sea Level Pressure reconstruction dataset (Cortesi et al., 2013); ERA40 reanalysis (Brisson et al., 2011)). Moreover, this methodology based in CWTs frequency is sufficiently simple to be applied to both past and future climates, thus providing a useful tool to quantify a measurable UI activity index for climates where we lack any direct upwelling activity records. In this context, this approach may be used to reconstruct the strength of upwelling indices since 1850 due to the existence of very high quality daily SLP dataset covering Europe and North Atlantic area. In fact, the authors have recently used a similar methodology to reconstruct monthly precipitation series for several Iberian stations (Cortesi et al., 2013).

Concerning climate change scenarios Lorenzo et al. (2011) studied the changes in future circulation types frequencies in Northwest Iberia Peninsula. Results show, in general, for the end of the 21st century (2081–2100 period) an increase in the NE circulation type along with a decrease in the frequency of Cyclonic, Western, and Southwestern circulation types in the spring and summer months. Taking into account the correlation obtained here, of the upwelling index with the NE circulation type frequency and the anti-correlation with the Cyclonic, Western, and Southwestern frequencies (see Sections 3.3 and 3.4) it is expectable to lead to an increase of favorable meteorological condition for upwelling in those months at least in the Northwest points that were studied (Rias Baixas and Aveiro). This result was also obtained by Miranda et al. (2012) using a high-resolution regional ocean model forced by future climate conditions, also at a regional scale. The same authors point out that one of the major difficulties in projecting future upwelling conditions is the models inability to reproduce winds in a fine-resolution grid. Although theoretically global warming would produce coastal wind stress strengthening because over-land thermal lows intensify due to a higher land–sea temperature difference, there are other factors that can attenuate or even reverse this effect, such as local ocean warming and changes in stratification. Di Lorenzo et al. (2005) observed that both factors work as a mechanism for the weakening of upwelling. On one hand, the warming of the ocean surface and upper levels will implicate an increase in stratification, which is unfavorable for vertical motion, and hence upwelling. On the other hand, coastal and offshore waters may undergo different warming rates due to the unequal temperature anomaly advection carried out by the mean coastal currents. This causes the deepening of the thermocline, enhancing further the inhibition effect on upwelling. That is, there are two opposite key factors at play in a warming scenario: an increase in upwelling-favorable winds, counteracted by upwelling-unfavorable stratification strengthening and/or deepening of the thermocline. The study of Di Lorenzo et al. (2005) seems to indicate the latter prevails over the former. Therefore, one must be careful in drawing conclusions concerning future upwelling changes based on changes in wind stress alone.

To conclude, with this methodology we present here and the proper sea level pressure fields even at lower resolution (5° by 5° grid is enough to compute the CWTs) it would be possible to construct long-term time series of UI, whether large-scale or synoptic and thus to infer upwelling activity in both centennial scale past and future climate scenarios. This would allow more assertive studies on the implications of climate change on marine ecosystems.

Acknowledgments

Alexandre M. Ramos was supported by the Portuguese Science Foundation (FCT) through a Postdoctoral Grant (SFRH/BPD/84328/2012). Ana Cordeiro Pires was supported by the Portuguese Science Foundation (FCT) through a Doctoral Grant (SFRH/BD/47500/2008).

The upwelling index 6-h time series were provided by Instituto Español de Oceanografía (www.indicedeafloramiento.ieo.es). The authors also acknowledge Gonzalo González-Nuevoa, from the Instituto Español de Oceanografía, for his support in providing the Upwelling index series.

The authors are indebted to the two reviewers for their helpful and constructive comments that helped to improve the manuscript.

References

Alvarez, I., Gomez-Gesteira, M., deCastro, M., Dias, J.M., 2008. Spatiotemporal evolution of upwelling regime along the western coast of the Iberian Peninsula. Journal of Geophysical Research 113, C07020, http://dx.doi.org/10.1029/2008JC004744.

Alvarez, I., Gómez-Gesteira, M., de Castro, M., Lorenzo, M.N., Crespo, A.J.C., Dias, J.M., 2011. Comparative analysis of upwelling influence between the western and northern coast of the Iberian Peninsula. Continental Shelf Research 31, 388–399.

Álvarez-Salgado, X.A., Rosón, G., Pérez, F.F., Pazos, Y., 1993. Hydrographic variability off the Rías Baixas (NW Spain) during the upwelling season. Journal of Geophysical Research 98 (C8), http://dx.doi.org/10.1029/93JC00458.

Arístegui, J., Barton, E.D., Álvarez-Salgado, X.A., Santos, A.M.P., Figueiras, F.G., Kifani, S., Hernández-León, S., Mason, E., Machú, E., Demarcq, H., 2009. Sub-regional ecosystem variability in the Canary Current upwelling. Progress in Oceanography 83, 33–48.

Bakun, A., 1973. Coastal Upwelling Indices, West Coast of North America, 1946–71. NOAA Tech. Rep., NMFS SSRF-671. U.S. Dep. Commer. 103 pp.

Bakun, A., 1990. Global climate change and intensification of coastal ocean upwelling. Science 247, 198–201.

Barton, E.D., Aristegui, J., Tett, P., Canton, M., Garcia-Braun, J., Hernandez-Leon, S., Nykjaer, L., Almeida, C., Almunia, J., Ballesteros, S., Basterretxea, G., Escanez, J., Garcia-Weill, L., Hernandez-Guerra, A., Lopez-Laatzen, F., Molina, R., Montero, M.F., Navarro-Perez, E., Rodriguez, J.M., van Lenning, K., Velez, H., Wild, K., 1998. The transition zone of the Canary Current upwelling region. Progress in Oceanography 41, 455–504.

Bograd, S.J., Schroeder, I., Sarkar, N., Qiu, X., Sydeman, W.J., Schwing, F.B., 2009. Phenology of coastal upwelling in the California Current. Geophysical Research Letters 36, L01602.

Borges, M.F., Santos, A.M.P., Crato, N., Mendes, H., Mota, B., 2003. Sardine regime shifts off Portugal: a time series analysis of catches and wind conditions. Scientia Marina 67, S1, http://dx.doi.org/10.3989/scimar.2003.67s1235.

Brisson, E., Demuzere, M., Kwakernaak, B., van Lipzig, N.P.M., 2011. Relations between atmospheric circulation and precipitation in Belgium. Meteorology and Atmospheric Physics 111, 27–39.

Cabanas, J.M., Alvarez, I., 2005. Ekman transport patterns in the area close to the Galician coast (NW, Spain). Journal of Atmospheric and Ocean Science 10 (4), 325–341.

Cortesi, N., Trigo, R.M., Gonzalez-Hidalgo, J.C., Ramos, A.M., 2013. Modelling monthly precipitation with circulation weather types for a dense network of stations over Iberia. Hydrology and Earth System Sciences 17, 665–678, http://dx.doi.org/10.5194/hess-17-665-2013.

Chavez, F.P., Messié, M., 2009. A comparison of eastern boundary upwelling ecosystems. Progress in Oceanography 83, 80–96, http://dx.doi.org/10.1016/j.pocean.2009.07.032.

deCastro, M., Gómez-Gesteira, M., Lorenzo, M.N., Alvarez, I., Crespo, A.J.C., 2008. Influence of atmospheric modes on coastal upwelling along the western coast of the Iberian Peninsula, 1985 to 2005. Climate Research 36, 169–179, http://dx.doi.org/10.3354/cr00742.

deCastro, M., Gómez-Gesteira, M., Álvarez, I., Crespo, A.J.C., 2011. Atmospheric modes influence on Iberian Poleward Current variability. Continental Shelf Research 31, 425–432.

Demuzere, M., Werner, M., van Lipzig, N.P.M., Roeckner, E., 2008. An analysis of present and future ECHAM5 pressure fields using a classification of circulation patterns. International Journal of Climatology 29 (12), 1796–1810, http://dx.doi.org/10.1002/joc.1821.

Di Lorenzo, E., Miller, A.J., Schneider, N., McWilliams, J.C., 2005. The warming of the California Current System: dynamics and ecosystem implications. Journal Physical Oceanography 35, 336–362, http://dx.doi.org/10.1175/JPO-2690.1.

Esteban, P., Jones, P.D., Martín-Vide, J., Mases, M., 2005. Atmospheric circulation patterns related to heavy snowfall days in Andorra, Pyrenees. International Journal of Climatology 25 (3), 319–329, http://dx.doi.org/10.1002/joc.1103.

Fiúza, A.F.G., Macedo, M.E., Guerreiro, M.R., 1982. Climatological space and time variation of the Portugal coastal upwelling. Oceanologica Acta 5 (1), 31–40.

Fiúza, A.F.G., 1983. Upwelling patterns off Portugal. In: Suess, E., Thiede, J. (Eds.), Coastal Upwelling. Its Sediment Record. Plenum, New York, pp. 85–98.

Fowler, H.J., Kilsby, C.G., 2002. Precipitation and the North Atlantic Oscillation: a study of climatic variability in northern England. International Journal of Climatology 22 (7), 843–866, http://dx.doi.org/10.1002/joc.765.

Frouin, R., Fiúza, A.F.G., Ambar, I., Boyd, T.J., 1990. Observations of a poleward surface current off the coasts of Portugal and Spain during winter. Journal of Geophysical Research 95 (C1), 679–691.

Gómez-Gesteira, M., deCastro, M., Álvarez, I., Lorenzo, M.N., Gesteira, J.L.G., Crespo, A.J.C., 2008. Spatio-temporal upwelling trends along the Canary upwelling system (1967–2006). Trends and Directions in Climate Research. Annals of the New York Academy of Sciences 1146, 320–337, http://dx.doi.org/10.1196/annals.1446.004.

Goodess, C.M., Palutikof, J.P., 1998. Development of daily rainfall scenarios for southeast Spain using a circulation-type approach to downscaling. International Journal of Climatology 18, 1051–1083.

Hamed, K.H., Ramachandra, A., 1997. A modified Mann–Kendall trend test for autocorrelated data. Journal of Hydrology 204, 182–196.

Haynes, R., Barton, E.D., 1990. A poleward flow along the Atlantic coast of the Iberian Peninsula. Journal of Geophysical Research 95 (C7), 425–441.

Haynes, R., Barton, E.D., Pilling, I., 1993. Development, persistence, and variability of upwelling filaments off the Atlantic Coast of the Iberian Peninsula. Journal of Geophysical Research 98 (C12), 681–692.

Hess, P., Brezowsky, H., 1952. Katalog der Großwetterlagen Europas. Berichte des Deutschen Wetterdienst in der US-Zone 33.

Hess, P., Brezowsky, H., 1977. Katalog der Grosswetterlagen Europas (1881–1976) Berichte des Deutschen Wetterdienstes. Nr. 113 Bd. 15, Selbstverlag des Deutchen Wetterdienstes, Offenbach am Main.

Hoinka, K.P., Castro, M., 2003. The Iberian Peninsula thermal low. Quarterly Journal of the Royal Meteorological Society 129 (590), 1491–1511, http://dx.doi.org/10.1256/qj.01.189.

Huth, R., Beck, C., Phillipp, A., Demuzere, M., Ustrnul, Z., Cahynová, M., Kyselý, J., Tveito, O.E., 2008. Classifications of atmospheric circulation patterns: recent advances and applications. Trends and Directions in Climate Research. Annals of the New York Academy of Sciences, 105–152, http://dx.doi.org/10.1196/annals.1446.019.

Jenkinson, A.F., Collison, F.P., 1977. An initial climatology of gales over the North Sea. Synoptic Climatology Branch Memorandum, 62, UK Met. Office, Bracknell. 18 pp.

Jones, P.D., Hulme, M., Briffa, K.R., 1993. A comparison of Lamb circulation types with an objective classification scheme. International Journal of Climatology 13, 656–663.

Jones, P.D., Lister, D.H., 2009. The urban heat island in Central London and urban-related warming trends in Central London since 1900. Weather, Royal Meteorological Society 64 (12), 323–327.

Kassomenos, P., 2010. Synoptic circulation control on wild fire occurrence. Physics and Chemestry of the Earth 35, 544–552, http://dx.doi.org/10.1016/j.pce.2009.11.008.

Kistler, R., Kalnay, E., Collins, W., Saha, S., White, G., Woollen, J., Chelliah, M., Ebisuzaki, W., Kanamitsu, M., Kousky, V., van den Dool, H., Jenne, R., Fiorino, M., 2001. The NCEP–NCAR 50-Year reanalysis: monthly means CD-ROM and documentation. Bulletin of the American Meteorological Society 82 (2), 247–268.

Kruizinga, S., 1979. Objective classification of daily 500 mbar patterns. In: Proceedings of Preprints Sixth Conference on Probability and Statistics in Atmospheric Sciences, Banff, Alberta. American Meteorological Society, Boston, MA, pp. 126–129.

Kysely, J., 2008. Influence of the persistence of circulation patterns on warm and cold temperature anomalies in Europe: analysis over the 20th century. Global and Planetary Change 62 (1–2), 147–163, http://dx.doi.org/10.1016/j.gloplacha.2008.01.003.

Lamb, H.H., 1972. British Isles weather types and a register of the daily sequence of circulation patterns, 1861–1971. Geophysical Memoires, HMSO London 116, 85.

Lavín, A., Diaz del Rio, G., Cabanas, J.M., Casas, G., 1991. Afloramiento en el Noroeste de la Peninsula Iberica. Indices de afloramiento para el punto 43° N 11° W. Periodo 1966–1989. Informes Técnicos del Instituto Español de Oceanografía. vol. 91, 40 pp.

Lavín, A., Diaz del Rio, G., Casas, G., Cabanas, J.M., 2000, Afloramiento en el Noroeste de la Peninsula Iberica. Indices de afloramiento para el punto 43° N 11° W. Periodo 1990-1999. Informes Técnicos del Instituto Español de Oceanografía. vol. 15, 25 pp.

Lemos, R.T., Pires, H.O., 2004. The upwelling regime off the west Portuguese coast, 1941–2000. International Journal of Climatology 24 (4), 511–524, http://dx.doi.org/10.1002/joc.1009.

Lorenzo, M.N., Ramos, A.M., Taboada, J.J., Gimeno, L., 2011. Changes in present and future circulation types frequency in Northwest Iberian Peninsula. PLoS ONE 6 (1), e16201, http://dx.doi.org/10.1371/journal.pone.0016201.

Macías, D., Franks, P.J.S., Ohman, M.D., Landry, M.R., 2012. Modeling the effects of coastal wind- and wind-stress curl-driven upwellings on plankton dynamics in the Southern California current system. Journal of Marine Systems 94, 107–119.

Miranda, P.M.A., Alves, J.M.R., Serra, N., 2012. Climate change and upwelling: response of Iberian upwelling to atmospheric forcing in a regional climate scenario. Climate Dynamics 40 (11-12), 2813–2824, http://dx.doi.org/10.1007/s00382-012-1442-9.

Narayan, N., Paul, A., Mulitza, S., Schulz, M., 2010. Trends in coastal upwelling intensity during the late 20th century. Ocean Sciences 6, 815–823, http://dx.doi.org/10.5194/os-6-815-2010.

Nykjaer, L., Van Camp, L., 1994. Seasonal and interannual variability of coastal upwelling along northwest Africa and Portugal from 1981 to 1991. Journal of Geophysical Research 99 (C7), http://dx.doi.org/10.1029/94JC00814.

Oliveira, P.B., Nolasco, R., Dubert, J., Moita, T., Peliz, A., 2009. Surface temperature, chlorophyll and advection patterns during a summer upwelling event off central Portugal. Continental Shelf Research 29, 759–774.

Paredes, D., Trigo, R.M., Garcia-Herrera, R., Trigo, I.F., 2006. Understanding precipitation changes in Iberia in early spring: weather typing and storm-tracking approaches. Journal of Hydrometeorology 7 (1), 101–113, http://dx.doi.org/10.1175/JHM472.1.

Pauly, D., Christensen, P., 1995. Primary production required to sustain global fisheries. Nature 374, 255–257.

Peliz, Á., Rosa, T.L., Santos, A.M.P., Pissarra, J.L., 2002. Fronts, jets, and counter-flows in the Western Iberian upwelling system. Journal of Marine Systems 35 (1–2), 61–77.

Pérez, F.F., Padín, X.A., Pazos, Y., Gilcoto, M., Cabanas, M., Pardo, P.C., Doval, M.D., Fatina-Busto, L., 2010. Plankton response to weakening of the Iberian coastal upwelling. Global Change Biology 16, 1258–1267, http://dx.doi.org/10.1111/j.1365-2486.2009.02125.x.

Philipp, A., Bartholy, J., Beck, C., Erpicum, M., Esteban, P., Fettweis, X., Huth, R., James, P., Jourdain, S., Kreienkamp, F., Krennert, T., Lykoudis, S., Michalides, S.C., Pianko-Kluczynska, K., Post, P., Rasilla Alvarez, D., Schiemann, R., Spekat, A., Tymvios, F.S., 2010. Cost733cat—a database of weather and circulation type classifications. Physics and Chemistry of the Earth 35, 360–373.

Philipp, A., Della-Marta, P.M., Jacobeit, J., Fereday, D.R., Jones, P.D., Moberg, A., Wanner, H., 2007. Long-term variability of daily North Atlantic–European pressure patterns since 1850 classified by simulated annealing clustering. Journal of Climate 20 (16), 4065–4095, http://dx.doi.org/10.1175/JCLI4175.1.

Prudhomme, C., Genevier, M., 2011. Can atmospheric circulation be linked to flooding in Europe? Hydrological Processes 25 (7), 1180–1190, http://dx.doi.org/10.1002/hyp.7879.

Queiroga, H., Cruz, T., dos Santos, A., Dubert, J., González-Gordillo, J.I., Paula, J., Peliz, A., Santos, A.M.P., 2007. Oceanographic and behavioural processes affecting invertebrate larval dispersal and supply in the western Iberia upwelling ecosystem. Progress in Oceanography 74, 174–191.

Ramos, A.M., Lorenzo, M.N., Gimeno, L., 2010. Compatibility between modes of low-frequency variability and circulation types: a case study of the northwest Iberian Peninsula. Journal of Geophysical Research 115, D02113, http://dx.doi.org/10.1029/2009JD012194.

Ramos, A.M., Ramos, R., Sousa, P., Trigo, R.M., Janeira, M., Prior, V., 2011. Cloud to ground lightning activity over Portugal and its association with circulation weather types. Atmospheric Research 101 (1–2), 84–101, http://dx.doi.org/10.1016/j.atmosres.2011.01.014.

Relvas, P., Barton, E.D., Dubert, J., Oliveira, P.B., Peliz, A., da Silva, J.C.B., Santos, A.M.P., 2007. Physical oceanography of the western Iberia ecosystem: latest views and challenges. Progress in Oceanography 74, 149–173.

Relvas, P., Luís, J., Santos, A.M.P., 2009. Importance of the mesoscale in the decadal changes observed in the northern Canary upwelling system. Geophysical Research Letters 36, L22601, http://dx.doi.org/10.1029/2009GL040504.

Roy, C., Reason, C., 2001. ENSO related modulation of coastal upwelling in the eastern Atlantic. Progress in Oceanography 49, 245–255.

Santos, A.M.P., Borges, M.F., Groom, S., 2001. Sardine and horse mackerel recruitment and upwelling off Portugal. Journal of Marine Sciences 58 (3), 589–596, http://dx.doi.org/10.1006/jmsc.2001.1060.

Santos, A.M.P., Kazmin, A.S., Peliz, A., 2005. Decadal changes in the Canary upwelling system as revealed by satellite observations: their impact on productivity. Journal of Marine Research 63, 359–379.

Santos, F., Gomez-Gesteira, M., deCastro, M., Alvarez, I., 2011. Upwelling along the western coast of the Iberian Peninsula: dependence of trends on fitting strategy. Climate Research 48, 213–218.

Sousa, P., Trigo, R.M., Aizpurua, P., Nieto, R., Gimeno, L., García-Herrera, R., 2011. Trends and extremes of drought indices throughout the 20th century in the Mediterranean. Natural Hazards and Earth System Sciences 11, 33–51.

Torres, R., Barton, E.D., 2007. Onset of the Iberian upwelling along the Galician coast. Continental Shelf Research 27, 1759–1778.

Torres, R., Barton, E.D., Miller, P., Fanjul, E., 2003. Spatial patterns of wind and sea surface temperature in the Galician upwelling region. Journal of Geophysical Research 108 (C4), 3130, http://dx.doi.org/10.1029/2002JC001361.

Trigo, R.M., DaCamara, C.C., 2000. Circulation weather types and their influence on the precipitation regime in Portugal. International Journal of Climatology 20 (13), 1559–1581, http://dx.doi.org/10.1002/1097-0088(20001115)20:13.

Vicente-Serrano, S.M., Lopez-Moreno, J.I., Gimeno, L., Nieto, R., Moran-Tejeda, E., Lorenzo-Lacruz, J., Begueria, S., Azorin-Molina, C., 2011. A multiscalar global evaluation of the impact of ENSO on droughts. Journal of Geophysical Research 116, D20109, http://dx.doi.org/10.1029/2011JD016039.

Wallace, J.M., Hobbs, P.V., 2006. Atmospheric Science. An Introductory Survey, second edition. Academic Press, UK.

Wilks, D.S., 2006. Statistical Methods in the Atmospheric Sciences. International Geophysics Series, Academic Press, USA.

Wooster, W.S., Bakun, A., McLain, D.R., 1976. Seasonal upwelling cycle along eastern boundary of North Atlantic. Journal of Marine Systems 34 (2), 131–141.

Yarnal, B., 1992. Synoptic Climatology in Environmental Analysis. Studies in Climatology Series, Belhaven Press, London, UK.